Session 2 - Unsteady Pressure Measurements

THE USE OF PIEZO RESISTIVE SEMI-CONDUCTOR PRESSURE TRANSDUCERS FOR FAST RESPONSE PROBE MEASUREMENTS IN TURBOMACHINERY

C. Gossweiler, H.J. Humm, P. Kupferschmied

ETH Zurich, Switzerland

1. Introduction

This paper describes the development of semiconductor-based high frequency response probe measurements. A family of single- and multi-sensor probes have been built using monocrystalline anisotropically etched silicon sensors. To enhance the accuracy of the pressure measurements, comprehensive investigations into the domain of sensor characterizing are currently performed at our laboratory. First results obtained from high subsonic diffuser flow in a radial compressor are presented.

2. Sensors

The piezoresistive pressure transducers, having been designed for biomedical applications, are manufactured by silicon micromachining. All its parts (resistors, interconnections and the insulating layers) are fabricated by a standard planar process like integrated circuits (KLOEK 1989; KAYAL/ANSERMET 1987). The forming of the membrane by anisotropic etching from the backside determines its orientation; thus its surface alignes with the (100)-plane of the silicon crystal. The resistors (boron doped p-type silicon with an inpurity concentration of $1 \cdot 10^{19}$ atoms/cm^3) are oriented in the (110)-direction. They are connected in a conventional Wheatstone-bridge configuration (see fig. 2.1). The resistors are fully passivated and electrically insulated from the substrate; they exhibit good overall stability and repeatability. With the precisely micromachined diaphragm and rigid chuck from solid, an accurate positioning of the resistors is feasible. Therefore good linearity and high sensitivity of the sensor results. Additionally the chuck acts as a rigid frame, and therefore a remarquable reduction of applied mechanical stress onto the membrane by packaging of the sensors is provided.

The sensitivity of the chips is approximately 20 µV/V/mbar. The diaphragm rupture pressure exceeds 20 bar. Typical chips used for our application measure 1 mm vs 2 mm, smallest 0.6 mm vs 1.5 mm, with a chip's thickness beetween 0.5 mm and 0.15 mm. Although the chips are batch-processed they show widely spread properties. Thus tests are routinely taken for all purchased sensors to evaluate whether they are appropriate for applications in our probes. These tests concern temperature coefficients of signal and excitation, stability and thermal hysteresis of the chip.

3. Sensor Packaging

Special attention has to be drawn to the packaging of the sensors. Most of the instabilities, thermal hysteresis and transient errors are considered to be caused by unproper packaging. These effects lead to inaccurate measurements in turbomachinery, especially if the DC-part of the signal is of interest.

Different arrangements in applying the sensors lead to a reduction of the above mentioned errors, mainly by:

- Choosing material of the probe's body matching the thermal expansion of the sensor chip closely (this was found to be a nickel alloy)
- Bonding the sensor to the probe using a rubberlike adhesive and therefore avoiding strain induced forces on the device (only possible for monolythic shaped sensors)

Environmental protection of the active silicon membrane is essential for applications in turbomachinery (fig. 5.3: wedge probe). An alternative method is given by the "backfaced" pressurisation, which does not require protection from the pressure medium but involves decreased but acceptable system's eigenfrequency due to an added pneumatic cavity (fig. 5.1: cylindrical probe).

4. Physical Properties of Sensors

After the packaging of the sensor into the probe further tests for sensor characterisation are required. The sum of the overall error can be expressed as the difference between the real quantity y(t) and the meashuring system output $\hat{y}(t)$:

$$e_{overall} = y(t) - \hat{y}(t) = e_{systematic} + e_{random} + e_{dynamic}$$

The main task is to quantify all errors and to most possibly compensate systematic errors. Calibrated pressure and temperature ranges where all relative errors refere to (Full Scale FS) are $0 \le p \le 1$ bar and $30 \le T \le 80$ °C.

4.1 Systematic Errors (static)

Typically for pressure sensors the systematic errors are due to their deviation from linearity and errors caused by temperature effects. Figure 4.2 shows calibration data U (p, T) and U_e (p, T), with U and U_e being signal and excitation voltage respectively.

If uncompensated, the errors amount to approximatively 0.5% FS deviation from linearity, temperature zero-shift 0.15% FS/K and temperature shift of span 0.15% FS/K with constant current excitation. Conventionally the bridge's shift and span would be compensated by adding external resistors to the bridge and thereby reducing the errors to 0.02% FS/K zero and 0.02% FS/K span holding the current excitation constant.

A model based reconstruction (MBR) seems to be an attractive approach to minimize systematic errors due to the ease with which it can be accomplished (fig. 4.1). The sensor's model (being polynomials) is provided by a series of static calibration data. The parameters of the model are obtained from a least-square approximation.

$$\hat{p} = \sum_{i}^{m} \sum_{j}^{n} c_{p\,ij} U^i U_E^j \qquad \hat{T} = \sum_{i}^{m} \sum_{j}^{n} c_{T\,ij} U^i U_E^j$$

The predicted values from the model $\hat{p}(U, U_E)$ and $\hat{T}(U, U_E)$ are plotted in figure 4.3. The number of parameters used for the modelling (normally less than 9) were optimized by applying Mallow's Cp-statistics (DANIEL/WOOD). The difference between calibraton data and corresponding predicted values from the model is called "reconstruction-error" (± 0.5 mbar over the whole calibration range) and is considered to be random (fig. 4.4)

4.2 Random Errors (static and dynamic)

The most significant random errors are due to drift, thermal hysteresis and long term stability. They can be considerably affected by packaging of the sensors. To a certain degree they can be reduced by recalibration of zero and span during the test period.

- The errors due to long term stability one year after calibration are 2.5 % FS (fig. 4.5)
- The thermal hysteresis of zero was found to be strongly dependent on the shape (amplitude, frequency) of the environmental temperature-cycle (max. ± 0.3 % FS for a one-week cycle).
- The electrical noise of the sensor (resistance & Shottky noise) and of the amplifier is bandwidth dependent and constraining to the system's resolution. For our setup the resolution is approximatively 10 Pa with a bandwidth of 40 kHz.

4.3 Dynamic Errors

Dynamic errors (caused by pressure and temperature transients) can exceed the previously described errors considerably. If not treated accordingly they prevent accurate measurements in turbomachinery.

Pressure Transients

Dynamic calibration of pressure transducers requires appropriate pressure generators. In general, the imposed input therefore may be either a periodic or a nonperiodic pressure signal with sufficient harmonic contents. In each case the dynamic properties of the transducer can be expressed as a function of the instrument's response to the input.

Shock Tube Experiments

Mechanical devices offer periodic pressure signals to a maximum frequency of 5 kHz (WEYER 1974). Although acoustic loudspeaker systems provide periodic signals with frequencies up to approximately 20 kHz, their amplitudes are too low for our applications.

The high frequency information is characteristic to shock waves generated in a shock tube with an almost perfect stepwise pressure rise. Dynamic calibration of pressure transducers can therefore be performed - approaching frequencies of 500 kHz (ENDEVCO TP 286, AINSWORTH e. a. 1989).

Due to the finite bursting time of the diaphragm, shock tubes often reveal a non-ideal behaviour. During the bursting period of the diaphragm, strong perturbations occur in the zone between diaphragm and compression wave. The shock tube configuration and the diaphragm material have been carefully optimized. Additionally for aerodynamic reasons, as the shock proceeds down the tube, this perturbation zone vanishes and the shape of the shock becomes steeper. Thus an almost perfect Heavyside step in pressure change arises (OERTL 1966).

Signal processing

The transfer function must be obtained from a known pair of associated input x(t) and output signals y(t) imposed and measured experimentally. In order to calculate the transfer function - which is expressed in the frequency domain - both input and output function have to be transformed accordingly. Fourier and Laplace analysis fulfil this requirement (SCHWEPPE e. a. 1967).

.

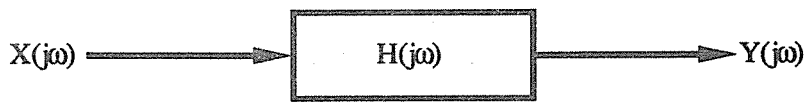

Hence the frequency response of the transducer can be determined

$$H(j\omega) = \frac{Y(j\omega)}{X(j\omega)}$$

Because of the lack of infinitely fast pressure transducers to measure the input signal correctly, the input signal is assumed to be an ideal step. Considering a delta function input, the transfer function can be written

$$H(j\omega) = Y(j\omega)$$

with $Y(j\omega)$ as the transformed transducer impulse response.

In the time domain the impulse response $y(t) = h(t)$ can be expressed as the derivative of the system step response u(t):

$$h(t) = \frac{d\,u(t)}{dt}$$

Thus the frequency response function is the Fourier transformed derivative of the sensor's normalized response to the shock wave impact.

Results

The investigations (GOSSWEILER/HUMM/KUPFERSCHMIED 1990) in the shock tube were performed using two different pressure transducers having circular diaphragms of Ø 0.7 mm corresponding to figure 4.6. The sensor Entran EPI 127 is flush-mounted, where the membrane of WDS 1026 sensor is recessed (0.5 mm).

The step response of the EPI 127 sensor is shown in figure 4.7. It reveals a resonance frequency of 575 kHz. A typical 2nd order behaviour with low damping rate can clearly be seen (Fig. 4.8). For this reason the sensor can be employed for measurements limited at 1/3 of its resonance frequency (~200 kHz). The Bode plot of the WDS 1026 (fig. 4.9) transducer reveals two peaks due to the eigenvibration of the membrane at 658 kHz and the influence of the pneumatic cavity at 100 kHz. The results illustrate, that small cavities may strongly affect the dynamic behaviour of the configuration.

Influence of pneumatic cavities

Tests were performed concerning the cavity's influence on signal behaviour by varying both the hole diameter D and screen thickness L (fig. 4.10). The resulting resonance frequency of the configuration can be determined either by a mathematical model based on a linear 1-D-theory (BERGH/TIJDEMAN 1965) or experimentally (fig.4.11). The discrepancies between theory and measurement are probably due to the fact that 3-D-effects were not taken into account in theory, as can be clearly seen from the slope of

the curves in figure 4.12: The higher the ratio L/D, the better the accordance between theory and experiment.

Thermal Transient Response

The susceptibility of aerodynamic probes to thermal transient effects is aggrevated by minimizing their dimensions, due to lacking thermal capacity when traversing a "cold" probe from a secure position into a running turbomachine. Although cooling of the probes offers improved thermal transient behaviour, this technique is for our probe-design beyond practical feasability.

Due to different thermal capacities and thermal expansion coefficients of the probe's components (sensor, adhesive, probe body) transient mechanical stress is applied to the devices when thermal shocks occur. Nonlinear elastic and plastic properties of the adhesives cause strongly nonlinear thermal transient response. Thus the thermal transfer function of the sensor is dependent on the input signal (temperature).

Experiments

Tests were performed to obtain a certain knowledge whether these described errors are prejudicial to the measurements. The imposed signals were either a temperature step from T_{min} to T_{max} or rectangular temperature pulses.The tests reveal no influence onto the sensor's sensitivity but zero of the bridge is affected.

Temperature and offset signal are shown in figure 4.13 from a sensor being exposed to a temperature pulse of 40 s length. The maximum deviation from zero can be seen amounting to 8.5 mbar (0,9 % FS per 50 K-pulse). The remaining offset decays to zero within 15 minutes. For a temperature step (upwards or downwards respectively) the maximum zero-shift is less than 20 mbar (2% FS/50 K-step).

5. Caracteristics of the Probes

5.1 Operative Range

The geometry of high frequency response pressure probes is essentially dictated - besides manufacturing aspects like probe casing firmness, sensor mounting or assembly tolerance - by the operative range of the probe. Our probe designs are derived from objectives like minimizing the probe's size (reduction of blockage effects and flow perturbations), increasing of spatial and time resolution and reducing the pneumatic cavity between the diaphragm of the sensor and the surrounding fluid to achieve a maximum frequency response. Furthermore, a high angular pressure response and well defined calibration curves are required. Tiny probe and stem dimensions are necessary to fit into experimental test rigs (both axial and radial machines); this is fulfilled satisfactory by our prismatic probe geometry. Some of these objectives are incompatible and have to be balanced.

5.2 Probe Geometry

The following pressure probe geometries have been designed and investigated:

- One-hole or four-hole cylindric probes for subsonic measurements
  Several different one-hole probes have been built (Ø 1.8 mm, see fig. 5.1), with which high frequency response measurements have been carried out in an automotive turbocharger and in a radial compressor test rig.

Four-hole probes (Ø 2.5 mm, fig. 5.2) were tested in highly turbulent airflows. They allow to determine the relevant unsteady flow vector both in magnitude and direction (total and static pressure, pitch and yaw angle, fluid temperature - and thus, Mach number).

- Two-hole wedge probes
  The two-hole wedge probes - designed for flow direction measurements in turbomachines at higher Mach numbers - are well adapted for the mounting of small pressure transducers (fig. 5.3) and show good aerodynamic properties at higher Mach numbers.

5.3 Aerodynamic Investigations

The discussed pressure probe types were built both in a fast response and in a conventional pneumatic version with the same geometry for aerodynamic tests. For this purpose, two wind channels were installed at the Laboratory:

- Free Jet Calibration Facility
  This wind channel (jet diameter 100 mm, see fig. 5.4) is adapted for probe calibration up to Mach 0.8.
- Supersonic Calibration Channel
  This channel (nozzle with cross-section 200 vs 40 mm, see fig. 5.5) is used for probe tests and calibration up to Mach 1.4. Holographic investigations of the flow field can be performed.

Both channels are equiped with the same airflow regulation system, a data acquisition system and a remote-controlled multi-axis probe traversing system which allows to rotate the probe in the airflow in well defined angular steps.

The pressure signals obtained during calibration under steady conditions (in function of stagnation pressure, pitch and yaw angle and Mach number) are transformed into dimensionless calibration coefficients and stored for computer evaluation of later unsteady measurements. Among other things, calibration coefficients must be well defined in the whole angle domain of the flow to obtain an adequate parametrisation of the calibration data. Typical calibration coefficients of our four-hole probe are shown in figure 5.6.

For the evaluation of fast response measurements steady calibration data was applied. This is only valid if the typical spatial scale of the flow structure exceeds the probe dimensions by a factor m. For $m >> 1$ quasi-steady flow conditions can be assumed. Future work at our laboratory will deal with this subject.

6. Measurement Equipement

The electric signals of the high frequency response sensors (embedded in the pressure probe or/and in wall taps) are measured, computed and stored in a specially developped data acquisition system. The 8 channel system, with a sampling rate up to 200 kHz per channel, constists essentially of following components (see Fig. 6.1):

- Amplifier:
  High signal-to-noise-ratio is required, as well as good frequency response
- Low-pass linear phase filter (anti-aliasing filter):
  Eight-pole Butterworth and allpass filter for phase correction. The obtained gain accuracy is about 1% up to 40 kHz
- Analog/digital-converter (resolution 12 bit, linearity 11.5 bit)

Two additional event bits for initiation reference can be set

- Memory system:
  During measurements, data is stored on-line into memory (RAM with total storage capacity of 32 MByte) and transfered afterwards to a hard-disk or a magnetic tape. The process is directed by the controller.

7. Data Evaluation

An open-ended, sofware-based system has been developped and implemented in a DEC VAX-environment to carry out the evaluation of measurement data. This system offers an easy-to-use user interface like VAX/VMS which allows to carry out the interpretation step by step with interactive commands. It is also possible to enlarge in a simple way the existing system with new functions or new procedures.

The most important features of the data evaluation system are:

- Efficient management and handling of the very large data sets, which are stored in the main frame memory during the processing in order to minimize I/O-time
- Data sorting and formatting facilities
- Conversion of measurement data into physical quantities according to electrical and aerodynamic calibration data
- Digital signal analysis, digital filtering, statistics (spectrum, correlation e. a.) and graphic output of the results are implemented, further routines can be flexibly embedded in the system.

8. Measurements

Tests were performed concerning the evolution of flow and pressure patterns in the stable and unstable diffuser's flow regime of a radial compressor test rig (HUNZIKER/ RIBI/SPIRIG/GYARMATHY 1990). The impeller (Ø 280 mm) is driven by a 440 kW DC-motor, diffuser width being 17 mm. The investigations were performed up to tip-speed Mach numbers of 0.75, thus a blade passing frequency of 6.5 kHz resulted.

The measurements comprised overall data, streamwise and circumferential wall pressure profiles as well as velocity and flow angle profiles near the diffuser inlet surveyed with small-size time-averaging or time-resolving probes. The AC-part of the signal was superposed to the time-averaged data.

8.1 Time-Averaged Measurements

Time-averaged flow field measurements were performed using a cylindrical two-hole probe (Ø 1.8 mm) at two different radii in the diffuser's entry region ($r/r_i = 1.05/1.16$). In a first step the time-averaged flow direction was determined; afterwards the total pressure was measured by aligning one hole facing the flow vector. The static pressure was measured with static wall taps on hub and casing; assuming the distribution between to be linear.

At low flow rate (MP70) the impeller yields an almost symmetric radial velocity profile $c_r(z)$ at the radius $r/r_i = 1.05$. By increasing the flow rate (MP78) the measurements revealed a thin boundary layer on the hub wall and a large flow deficit on the casing side. Towards larger radii ($r/r_i = 1.16$) the flow deficit is accentuated, but still no reverse flow can be observed (fig. 8.1).

The flow angles fairly comply with the blade's outlet angle (60° from peripheral) in the core region only.

8.2 Fast Response Measurements

A cylindrical probe (Ø 1.8 mm) equiped with a miniature pressure sensor was traversed at the previously described radii. To avoid superposed fluctuations on the signals (rotating stall or mild surge), the measurements were limited to stable operational points of the compressor.

By sampling the data with the same initiation reference over a time interval much longer than the characteristic signal periode and followed averaging of corresponding digitized signals, any stochastic signal components were eliminated. In order to record the time-dependent total-pressure of the flow, the fast response probe was aligned, its hole facing the time-averaged direction of the flow to be examined.

Within a flow vector deviation of about ± 8° from the nulled angle, total pressure can be measured with less than 1 % of error (fig. 8.2: stationary calibration data). For deviations of ± 15° the probe still reads more than 95 % of the dynamic head. The fluctuation of static pressure was obtained from flush mounted wall-pressure sensors.

By yawing the same probe equiped with only one hole alternatively 45° in each direction and hence applying stationary calibration data (fig. 8.3), a rough determination of the instationary flow angle was feasible. When assuming the coefficient $c_p(\beta)$ to be linear over a range of $-15° < \beta < 15°$ and determining the flow angle:

$$\beta = \Delta c_{p12} \frac{dc_{p12}}{d\beta}$$

a maximum error of ± 0.5° occurs. An investigation by GROH 1989 - using potential-flow theory applied to the vaneless diffuser - concerning the influence of radial pressure gradients and velocity gradients on the cylindrical probe yaw-measurements was performed. The results show that these effects counterbalance each other.

Results

The shaded areas represent regions where the radial component is less then 90% of the momentum-averaged time-mean velocity (fig. 8.4) By comparing part a and b of the figure (high flow rate versus low flow rate), the change of the distribution of the deficit area is apparent: at high flow rate the deficit flow "accumulates" at the casing wall; at lower rates (beginning of instability) distinctive jet-wake flow can be observed. By changing the radial position from $r/r_i = 1.05$ to 1.16 (part b and c respectively), a certain migration of the deficit area towards the hub side of the diffuser occurs. Results of the angular fluctuation can be seen in fig. 8.5.

9. Conclusion/Outview

Measurements revealed a high reliability of the system. Although no protective layer was applied to the membrane's surface, lifetime of the devices exceeded 100 hours in strongly turbulent airflows at Mach numbers up to 0.75.

By further improvement of the sensor packaging and by better quantifying of its inherent errors, accurate measurements of the signal's DC-part seem to be within reach.

10. Acknowledgements

This work is supported by the Swiss Government (Schweizerischer Nationalfonds zur Förderung der wissenschaftlichen Forschung).

The authors would like to express their sincere appreciation to Prof. G. Gyarmathy, Mr. R. Hunziker, B. Ribi, M. Spirig for making available the presented results from the test rig, Mr. N. O. Chrisander for his software development and to Dr. G. Groh for his theoretical work.

Literature

AINSWORTH, R.W.; ALLEN,J.L.; DIETZ, A.J.
Methodes for making unsteady aerodynamic pressure measurments in a rotating turbine stage
AGARD Conf. preprint No. 468 ccp - 468
Luxembourg 1989

BERGH, H.; TIJDEMAN, H.
Theoretical and experimental results for the dynamic response of pressure measuring systems
NLR - TR F.283 1965

DANIEL C., WOOD F.
Fitting equations to data
Wiley Interscience New-York 1971

ENDEVCO TECH. PAPER TP 286

GOSSWEILER C., HUMM H.J., KUPFERSCHMIED P.
Proceedings of Micromechanics Europe 1990
Berlin November 1990

GROH G.
Zylindersonde in Spiralströmung
Internal report TN-LSM-89-10
ETH Zurich, Turbomachinery Laboratory 1989

HUNZIKER R., RIBI B., SPIRIG M., GYARMATHY G.
On the influence of different impellers on a radial compressor stage with vaneless diffuser
Interfluid Essen (FRG) 1990

KAYAL A.H., ANSERMET S., BUI N.C.
Mecano-microelectronic silicon transducers
Proceedings of Mechatronic-Symposium 1987

KLOECK B.
Design, fabrication and characterisation of piezorestive pressure sensors, including the study of electrochemical etch-stop
PhD-Thesis Université de Neuchâtel 1989

OERTL, H.
Stossrohre
Springer 1966

SCHWEPPE, J.L.; EICHBERGER, L.C.; MUSTER, D.F.; MICHAELIS, E.L.; PASKUSZ, G.F.
Methods for the dynamic calibration of pressure transducers
National Bureau of Standards Monograph 67 1967

WEYER, H.
Bestimmung der zeitlichen Druckmittelwerte in stark fluktuierender Strömung, insbesondere in Turbomaschinen
Diss. TH Aachen 1974

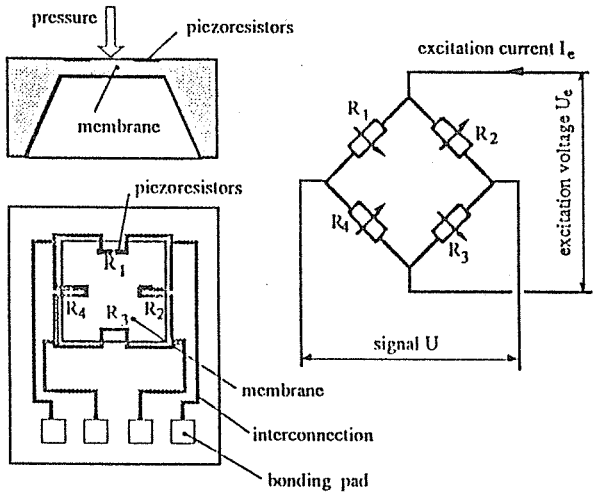

Figure 2.1 : sensor chip

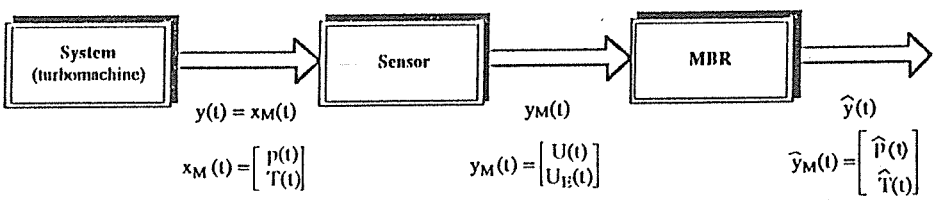

Figure 4.1 : model-based reconstruction

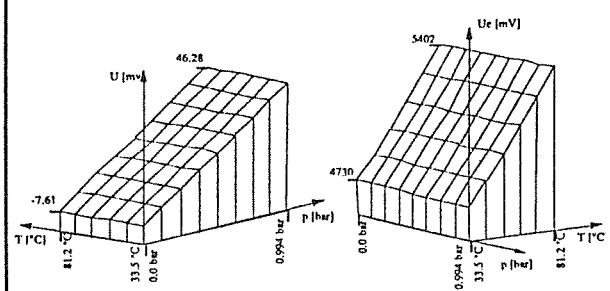

Figure 4.2 : calibration data of a sensor in the range $0 \le p \le 1$bar; $30 \le T \le 80$°C.

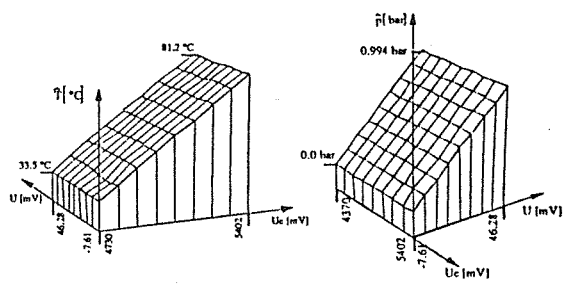

Figure 4.3 : predicted values from sensor model

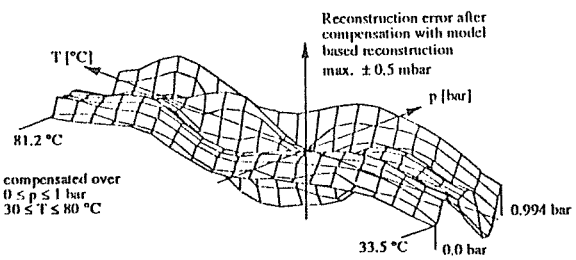

Figure 4.4 : reconstruction error

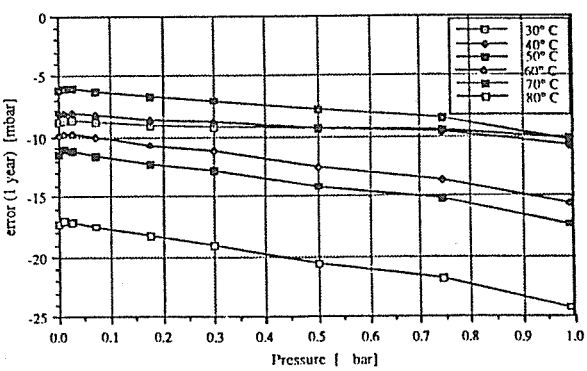

Figure 4.5 : long term stability (errors one year after calibration)

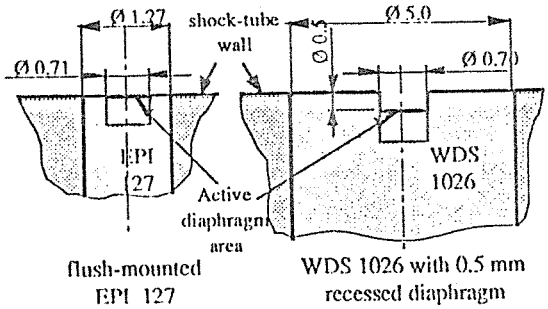

Figure 4.6 : pressure transducers ENTRAN EPI 127 and WDS 1026 (KELLER 1026 sensor)

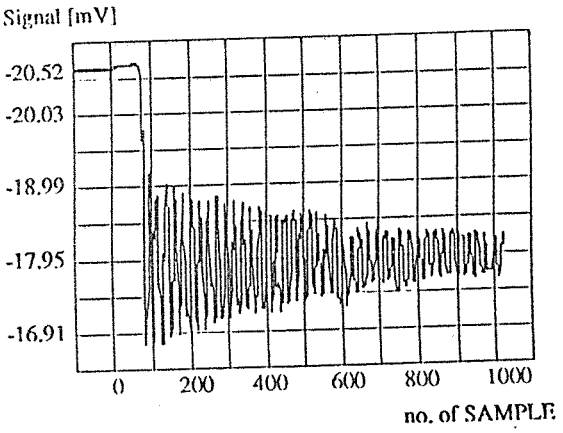

Figure 4.7 : step response of ENTRAN EPI 127

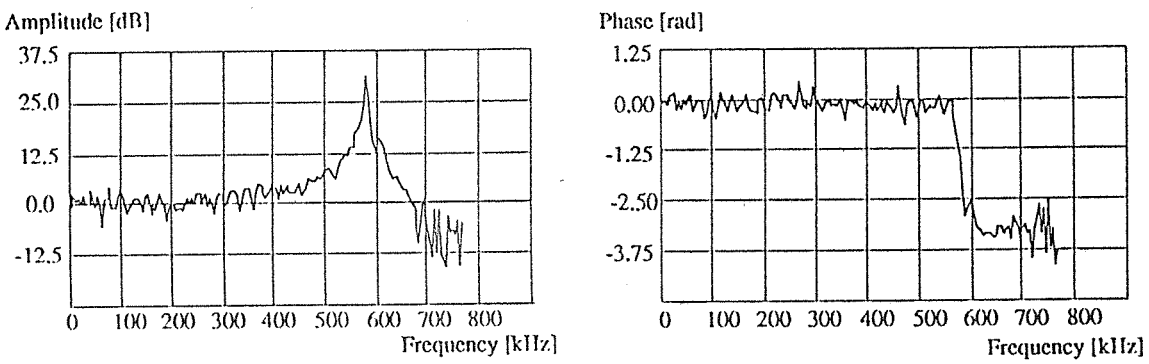

Figure 4.8 : Bode plot of ENTRAN EPI 127

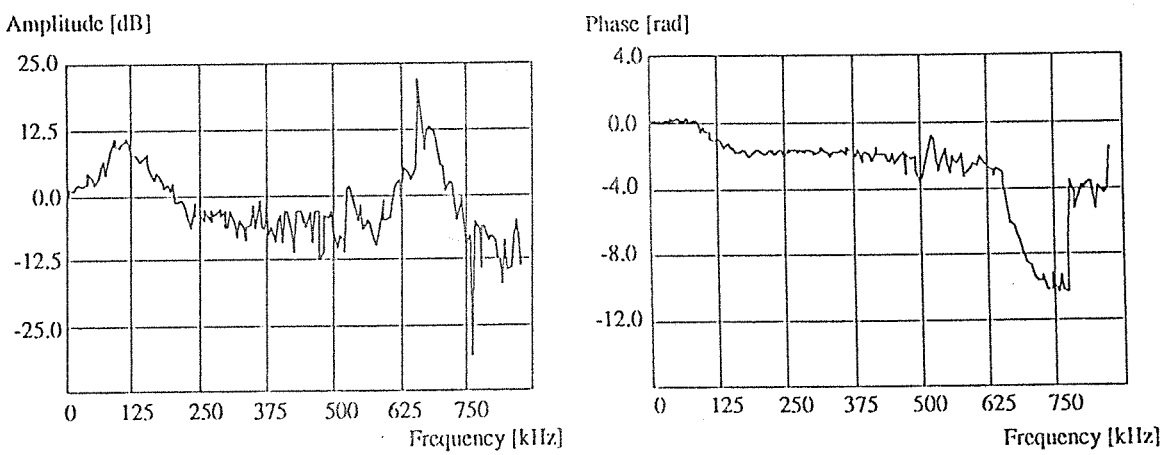

Figure 4.9 : Bode plot of WDS 1026

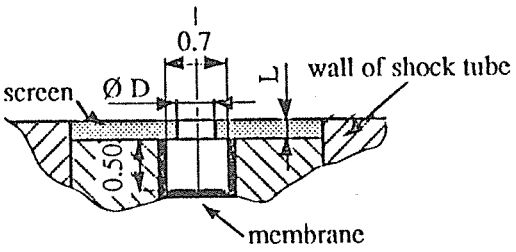

Figure 4.10 : screen configuration of WDS 1026

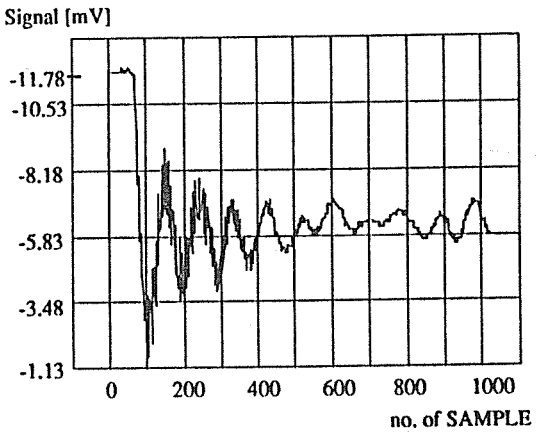

Figure 4.11 : step response with screen
D = 0.395 mm, L = 0.286 mm
duration 200 µs

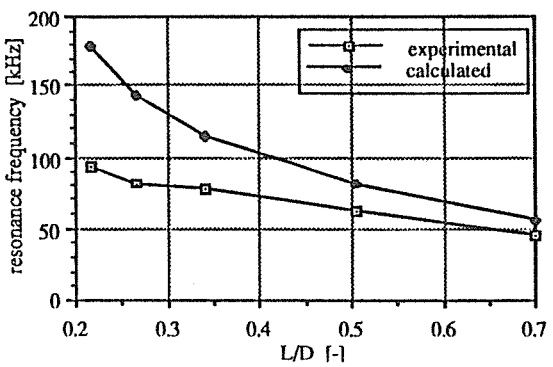

Figure 4.12 : resonance frequency with
different screens
L = 0.14mm = constant

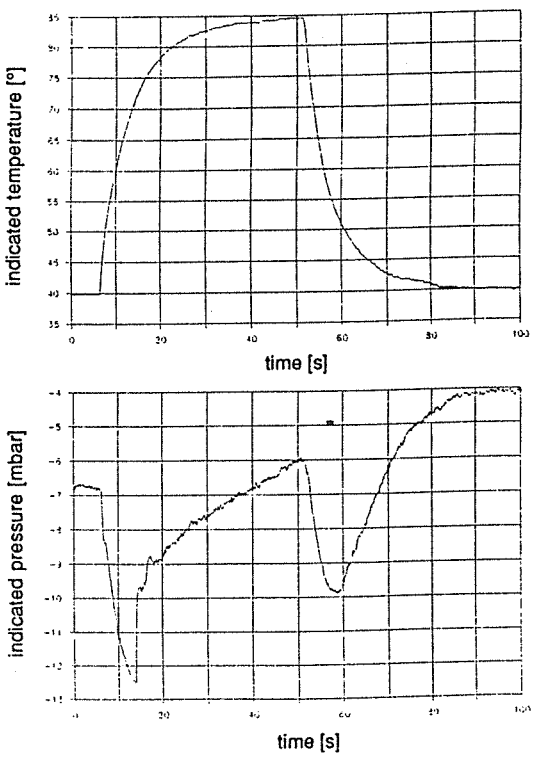

Figure 4.13 : thermal transient tests

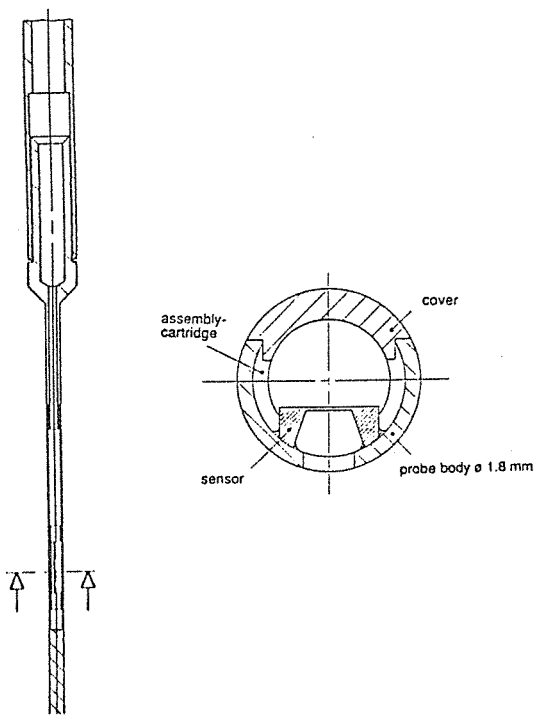

Figure 5.1 : one-hole cylindrical probe Ø 1.8 mm

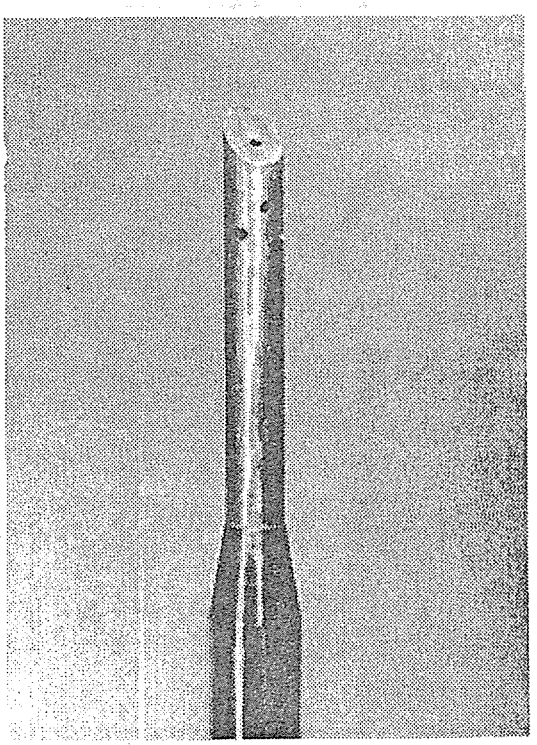

Figure 5.2 : four-hole cylindrical probe Ø 2.5 mm

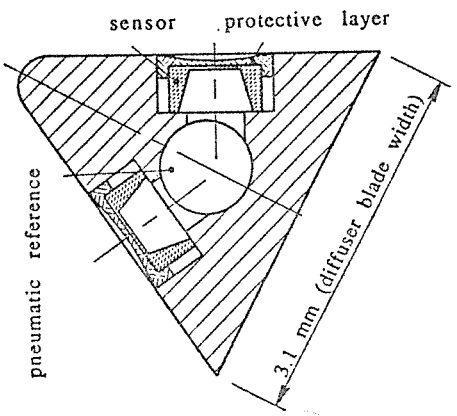

Figure 5.3 : two-hole wedge probe

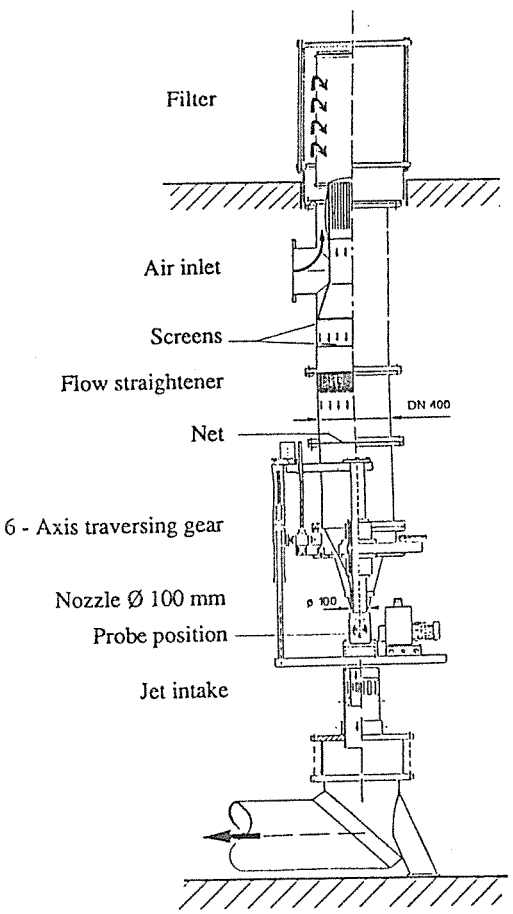

Figure 5.4 : free-jet calibration facility

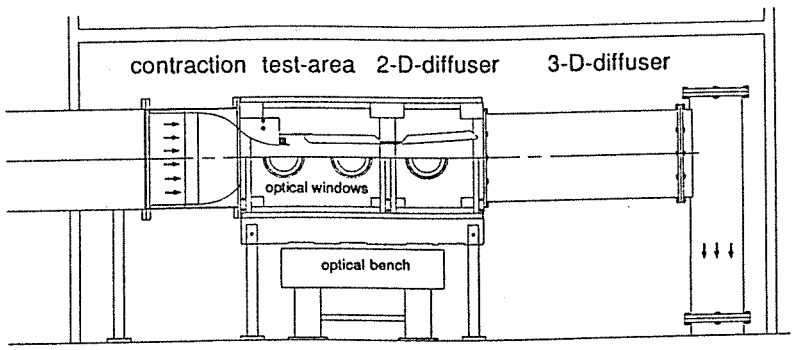

Figure 5.5 : supersonic calibration channel (subsonic setup)

$$K_1 = \frac{p_1 - p_4}{p_1 - \frac{p_2 + p_3}{2}}$$

$$K_2 = \frac{p_{tot} - p_1}{p_1 - \frac{p_2 + p_3}{2}}$$

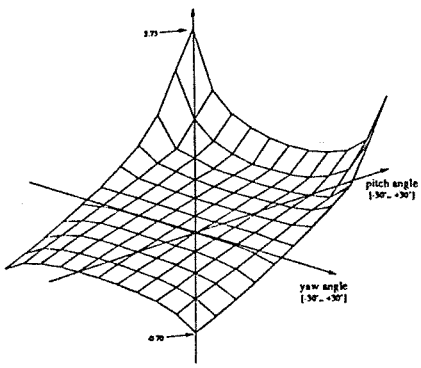

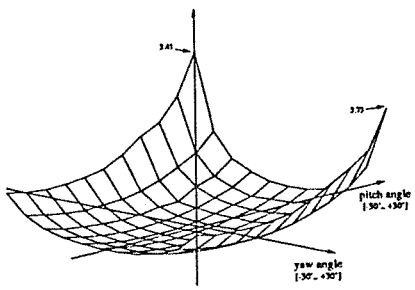

$$K_3 = \frac{p_{tot} - p_{stat}}{p_1 - \frac{p_2 + p_3}{2}}$$

$$K_4 = \frac{p_2 - p_3}{p_1 - \frac{p_2 + p_3}{2}}$$

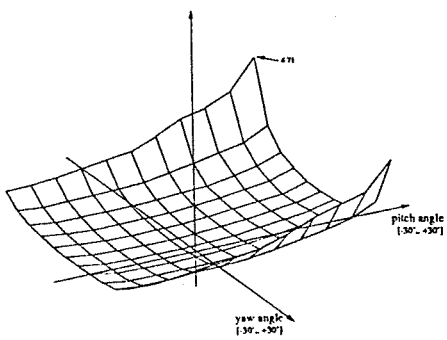

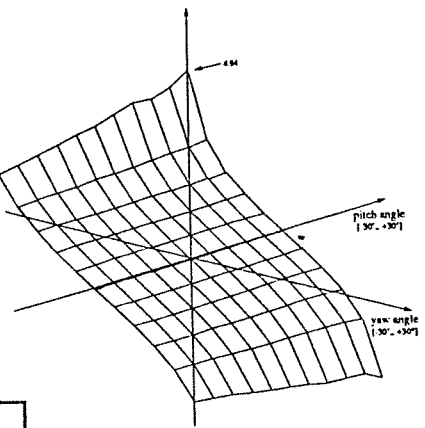

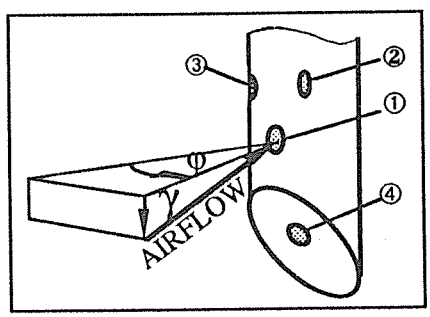

Figure 5.6 : calibration coefficients of four-hole cylindrical pressure probe

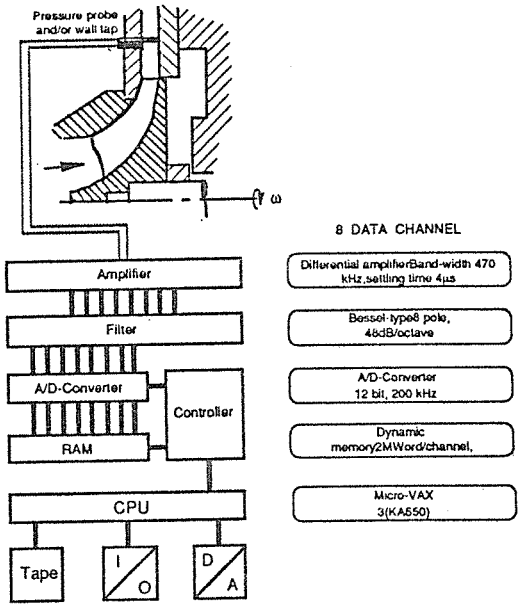

Figure 6.1 : high frequency response measurement and data acquisition

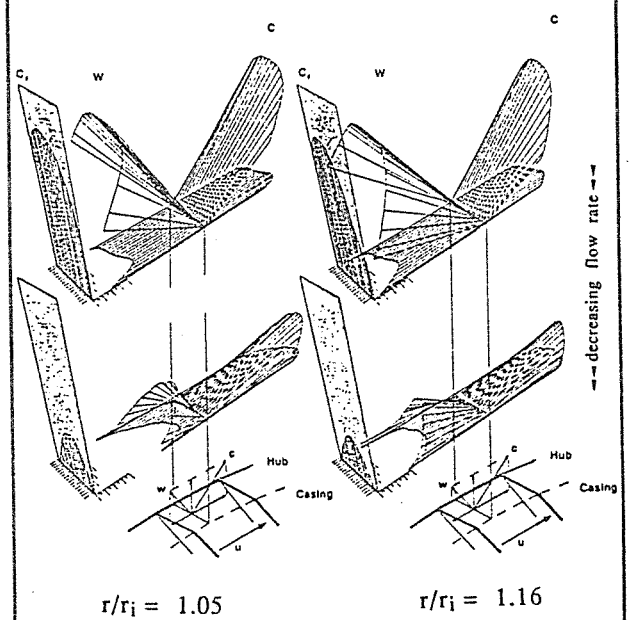

Figure 8.1 : time averaged flow measurements

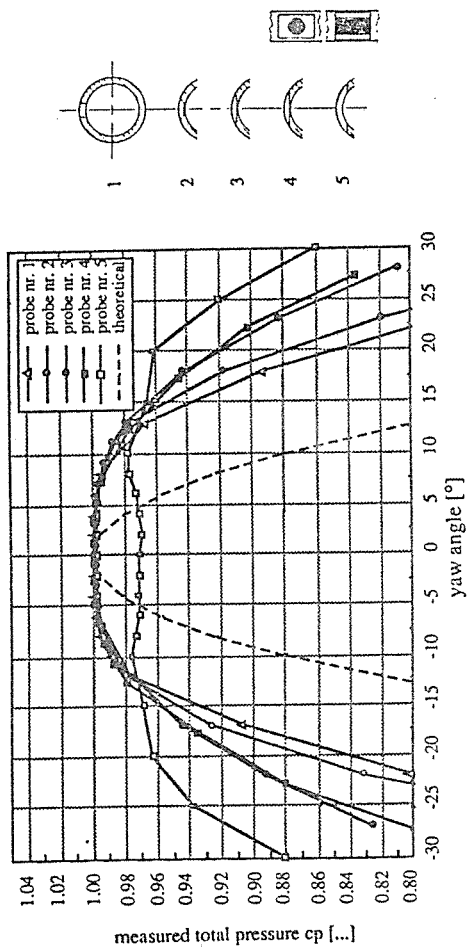

Figure 8.2 : non-dimensional calibration data

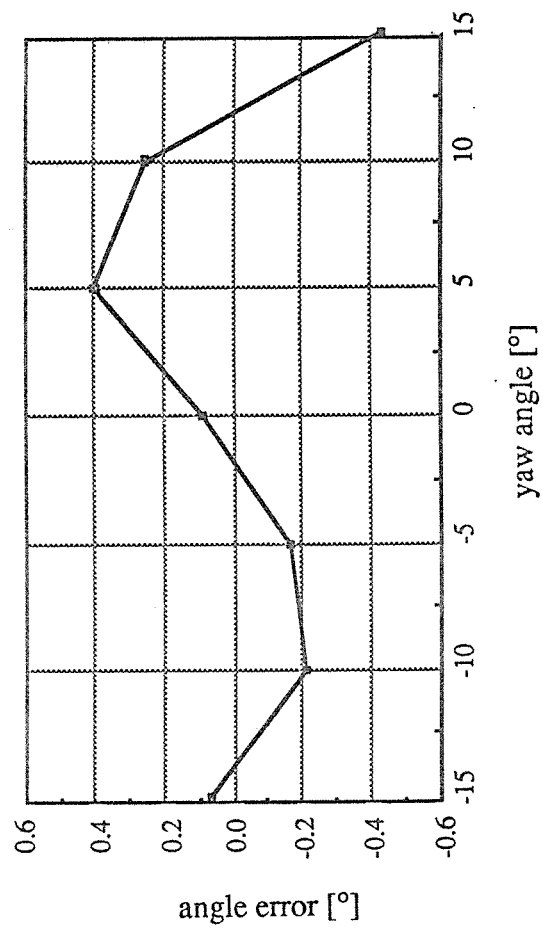

Figure 8.3 : angle error due to linearized calibration data

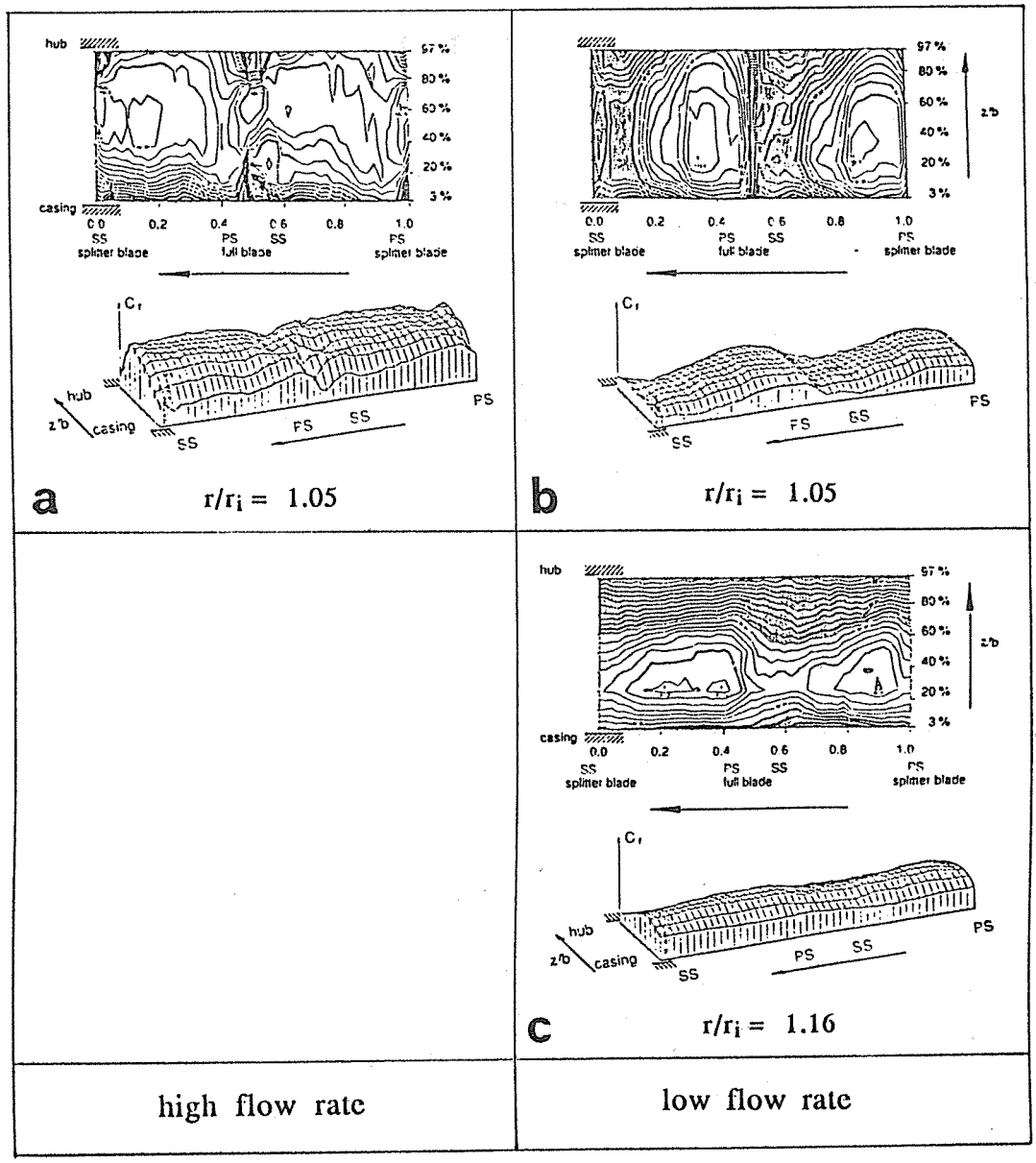

Figure 8.4 : fast response measurements

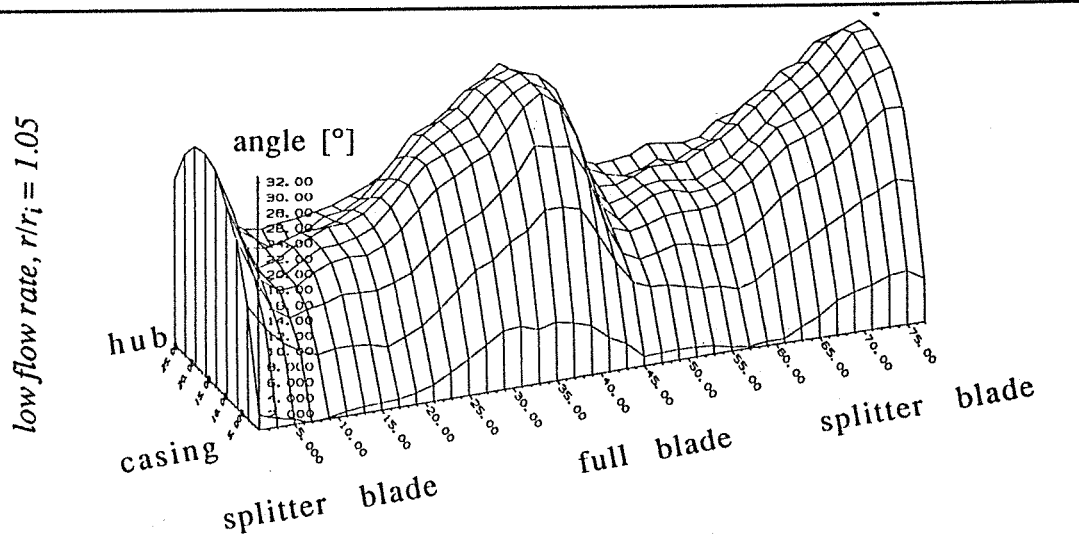

Figure 8.5 : fluctuation of flow angle